Development and comparison of the DTM, the DOM and the FVM formulations for the short-pulse laser transport through a participating medium

Subhash C. Mishra [a,*], Pranshu Chugh [a], Pranav Kumar [a], Kunal Mitra [b]

[a] *Department of Mechanical Engineering, Indian Institute of Technology Guwahati, Guwahati 781 039, India*
[b] *Department of Mechanical and Aerospace Engineering, Florida Institute of Technology, 150 West University Boulevard, Melbourne, FL 32901-6975, USA*

Abstract

The present article deals with the analysis of transient radiative transfer caused by a short-pulse laser irradiation on a participating medium. A general formulation of the governing transient radiative transfer equation applicable to a 3-D Cartesian enclosure has been presented. To solve the transient radiative transfer equation, formulations have been presented for the three commonly used methods in the study of radiative heat transfer, viz., the discrete transfer method, the discrete ordinate method and the finite volume method. To show the uniformity in the formulations in the three methods, the intensity directions and the angular quadrature schemes for computing the incident radiation and heat flux have been taken the same. To validate the formulations and to compare the performance of the three methods, effect of a square short-pulse laser having pulse-width of the order of a femtosecond on transmittance and reflectance signals in case of an absorbing and scattering planar layer has been studied. Effects of the medium properties such as the extinction coefficient, the scattering albedo and the anisotropy factor and the laser properties such as the pulse-width and the angle of incidence on the transmittance and the reflectance signals have been compared. In all the cases, results of the three methods were found to compare very well with each other. Computationally, the discrete ordinate method was found to be the most efficient.
© 2005 Elsevier Ltd. All rights reserved.

1. Introduction

In the recent past, research on the application of transient radiative heat transfer in participating media has gained a momentum. This owes to the availability of short-pulse lasers combined with the rapid development in electronics to analyze the signals having temporal variations of the order of a femtosecond to a picosecond. Applications of short-pulse laser transport in participating media include, but are not limited to, optical tomography of tissues [1–4], remote sensing of oceans and atmospheres [5–7], laser material processing of microstructures [8–10] and particle detection and sizing [11]. A detailed review dealing with various aspects of the transient radiative

transfer caused by the irradiation of short-pulse lasers has been given by Kumar and Mitra [10].

To analyze radiative transport problems involving steady-state diffuse and/or collimated radiation, more than a dozen methods are available [12,13]. Depending upon the medium types, geometries involved and its application in the presence of other modes of heat transfer, each method has some strong and weak points [12,13]. However, among the available methods, the discrete transfer method (DTM) [14], the discrete ordinate method (DOM) [15] and the finite volume method (FVM) [16] are extensively used for the transient or the steady-state conjugate mode (radiation, conduction and/or convection) heat transfer problems in which transport of radiation is considered to be a steady-state process [12,13].

In the present decade, with the start of research in area of transient radiative transfer, applications of various

* Corresponding author. Tel.: +91 361 2582660; fax: +91 361 2690762.
  E-mail address: scm_iitg@yahoo.com (S.C. Mishra).

Nomenclature

A	area	η	direction cosine with respect to the z-axis
a	anisotropy factor	σ	Stefan–Boltzmann constant $= 5.67 \times 10^{-8}$ W/m^2 K^4
c	speed of light		
G	incident radiation	σ_s	scattering coefficient
H	Heaviside function	τ	optical depth
I	intensity	Ω	direction, (θ, ϕ)
I_b	blackbody intensity, $\frac{\sigma T^4}{\pi}$	$\Delta\Omega$	solid angle, $\sin\theta\, d\theta\, d\phi$
$\hat{i}, \hat{j}, \hat{k}$	unit vectors in x-, y-, z-directions, respectively	ω	scattering albedo $(= \frac{\sigma_s}{\beta})$
M	number of discrete directions	ϕ	azimuthal angle
p	scattering phase function		
$\hat{n}$	outward normal	*Subscripts*	
q	heat flux	av	average
r	position	0	for collimated radiation
S	source term	c	collimated
s	geometric distance in the direction of the intensity	d	diffuse
		E, W, N, S, F, B	east, west, north, south, front, back
T	temperature	w	wall/boundary
t	time	e	exit
t_p	pulse-width	i	inlet
V	volume of the cell	P	cell centre
X, Y, Z	dimensions of the 3-D rectangular enclosure	ref	reflectance
x, y, z	Cartesian coordinate directions	s	start
		x, y, z	for x-, y-, z-faces of the control volume
Greek symbols		t	total
α	finite-difference weighing factor	tr	transmittance
β	extinction coefficient $(= \kappa_a + \sigma_s)$		
δ	Dirac-delta function	*Superscripts*	
κ_a	absorption coefficient	D	downstream point
μ	direction cosine with respect to the x-axis	m	index for the discrete direction
ε	emissivity	U	upstream point
θ	polar angle	*	dimensionless quantity
ξ	direction cosine with respect to the y-axis		

radiative transfer methods were extended to transient studies [17–31]. Kumar et al. [17], Mitra et al. [18] used the P-1 approximation to model the transient radiative transfer in 1-D and 2-D rectangular enclosures. Integral equation formulation was used by Tan and Hsu [19,20] and Wu and Wu [21]. Wu and Ou [22] applied the differential approximation to analyze the problems. The Monte Carlo method was used to model the transient radiative transfer by Schweiger et al. [23] and Guo et al. [24,25]. Guo and Kumar [26] and Sakami et al. [27] extended applications of the DOM to the 2-D rectangular enclosure. Application of the DOM to the 3-D rectangular enclosure was extended by Guo and Kumar [28]. Rath et al. [29] used the DTM to study the transient radiative transfer process in a planar medium. Their results compared very well with those of the DOM and the integral equation formulation. The application of the radiation element method to study the transient radiative transfer in various rectangular geometries was extended by Guo and Kumar [30]. The FVM was applied to study the short-pulse laser

transport in participating media by Chai [31] and Chai et al. [32].

A comparative study of the four methods, viz., the P-N approximation, the two-flux, the DOM and the direct numerical integration methods in predicting transient radiative transfer in a planar medium was done by Mitra and Kumar [33]. They showed that all methods do not predict the wave propagation speeds correctly. Wu and Ou [22] compared the modified differential approximations, the integral equation formulation and the modified P-1 approximation in the study of a planar medium. They found good agreements between differential approximations and the integral equation formulation.

It has been pointed above that the DTM, the DOM and FVM are the widely used methods in analysis of thermal problems in which radiation is considered to be in the steady-state, and recently these methods have also been applied to transient radiative transfer. However, as far as comparison of these methods is concerned, no study has been performed so far to check the accuracy and

computational efficiency of one over the other. The present work is, therefore, aimed at comparing the results and the computational efficiencies of these three popular methods for various parameters. In the literature, the formulations of these methods, for the steady [12,13] as well as for transient [26–32] states are presented in a manner which seem to be entirely different. One other objective of the present article is thus also to present a general formulation in which in the three methods the same intensity directions, expressions for the source terms and the quadratures for the angular integrations of the incident radiation and heat flux can be used. Further, the ray tracing algorithms in the DOM and the FVM are also exactly the same. The only difference between the two methods being that in the FVM unlike the DOM, intensity over an elemental solid angle is not considered isotropic. The ray tracing procedures in the DTM is different from those of the DOM and the FVM. However, for the transient study, the time marching procedure in the three methods is the same.

To validate the formulations in the DTM, the DOM and the FVM, effect of a square short-pulse laser irradiation on transmittance and reflectance signals from a planar medium has been studied and compared. These comparisons have been made for the effects of the extinction coefficient, the scattering albedo, the anisotropy factor, the angle of incidence and the pulse-width of the laser irradiation. CPU times in the three methods have also been compared.

2. Formulation

Let us consider an absorbing, emitting and scattering three-dimensional medium as shown in Fig. 1. Its north boundary is subjected to a collimated radiation I_c at an angle Ω_0. The radiation pulse I_c at this boundary is available only for a duration t_p which is of the order of a nano-second. The incident radiation pulse travels with the speed of light c, and at any location in the medium, it remains available for the duration of the pulse-width t_p (Fig. 2). Since the medium is participating and the bound-
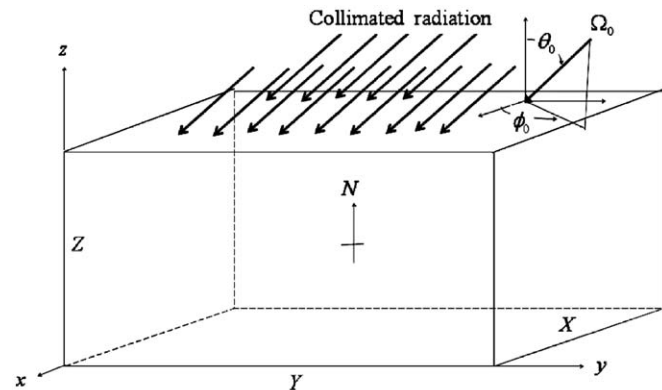

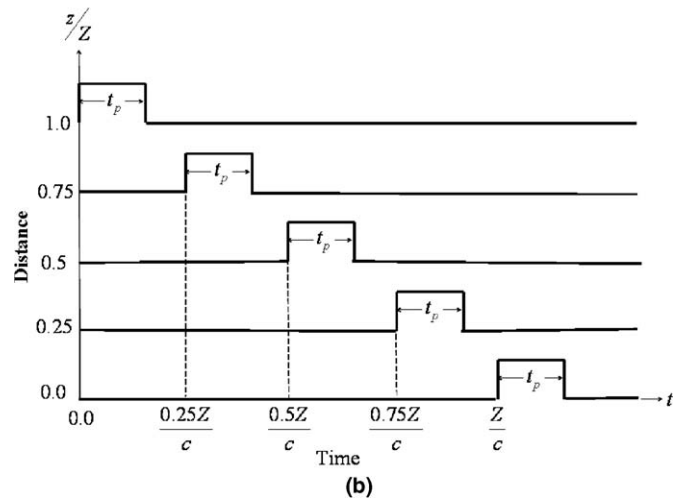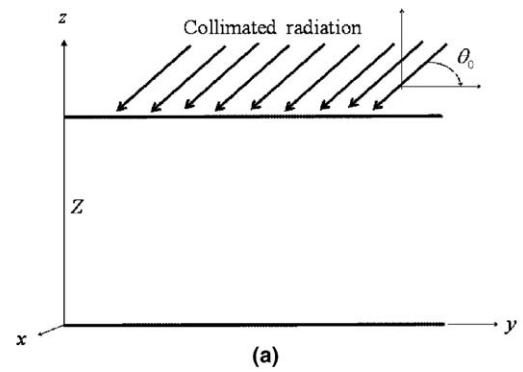Fig. 1. A 3-D rectangular geometry and the coordinates under consideration.

Fig. 2. (a) A planar medium subjected to collimated square pulse irradiation at its top boundary. (b) Time of arrival of the collimated square pulse at different locations in a planar medium for a normal angle of incidence, $\theta_0 = 0°$.

aries are at finite temperatures, the diffuse radiation also becomes time dependent. In this situation, the radiative transfer equation (RTE) in any direction $\hat{s}$ identified by the angle Ω about the elemental solid angle $\Delta\Omega$ is given by [12]

$$\left(\frac{1}{c}\right)\frac{\partial I}{\partial t} + \frac{dI}{ds} = -\beta I + \kappa_a I_b + \frac{\sigma_s}{4\pi}\int_{4\pi} Ip(\Omega, \Omega')\,d\Omega' \qquad (1)$$

where s is the geometric distance in the direction $\hat{s}$, k_a is the absorption coefficient, β is the extinction coefficient, σ_s is the scattering coefficient and p is the scattering phase function.

In Eq. (1), the intensity I within the medium is composed of two components, viz., the collimated intensity I_c and the diffuse intensity I_d.

$$I = I_c + I_d \qquad (2)$$

The variation of the collimated component I_c within the medium is given by [12]

$$\frac{dI_c}{ds} = -\beta I_c \qquad (3)$$

Substituting Eqs. (2) and (3) in Eq. (1) yields

$$\left(\frac{1}{c}\right)\frac{\partial I_c}{\partial t} + \left(\frac{1}{c}\right)\frac{\partial I_d}{\partial t} + \frac{dI_d}{ds}$$
$$= -\beta I_d + \kappa_a I_b + \frac{\sigma_s}{4\pi}\int_{4\pi} I_d p(\Omega, \Omega')\,d\Omega'$$
$$+ \frac{\sigma_s}{4\pi}\int_{4\pi} I_c p(\Omega, \Omega')\,d\Omega' \qquad (4)$$

Eq. (4) can be written as

$$\left(\frac{1}{c}\right)\frac{\partial I_c}{\partial t} + \left(\frac{1}{c}\right)\frac{\partial I_d}{\partial t} + \frac{dI_d}{ds} = -\beta I_d + S_c + S_d = -\beta I_d + S_t \qquad (5)$$

where S_c and S_d are the source terms resulting from the collimated and the diffuse components of radiation, respectively. In Eq. (5), $S_t = S_c + S_d$ is the total source term.

At any point in the medium, the collimated radiation I_c remains available only for the pulse duration t_p. For a square pulse, the value of I_c remains constant during the time duration t_p and zero at other times. Thus the time derivative of I_c becomes zero (this fact can be understood with the help of the illustration given in Fig. 2 for a planar medium). Eq. (5) can then be written as

$$\left(\frac{1}{c}\right)\frac{\partial I_d}{\partial t} + \frac{dI_d}{ds} = -\beta I_d + S_t \qquad (6)$$

The source term S_c resulting from the collimated radiation I_c is given by

$$S_c(t) = \frac{\sigma_s}{4\pi}\int_{\Omega'=0}^{4\pi} I_c(\Omega, t)p(\Omega, \Omega')\,d\Omega' \qquad (7)$$

For a linear anisotropic phase function $p(\Omega, \Omega') = 1 + a\cos\theta\cos\theta'$, the source term S_c is given by

$$S_c(t) = \left(\frac{\sigma_s}{4\pi}\right)\int_0^{2\pi}\int_0^{\pi} I_c(\theta, \phi, t)(1 + a\cos\theta\cos\theta_0)\sin\theta\,d\theta\,d\phi \qquad (8)$$

where θ and ϕ are the polar and azimuthal angles, respectively. In terms of the incident radiation G and heat flux q, Eq. (8) can be written as

$$S_c(t) = \frac{\sigma_s}{4\pi}[G_c(t) + a\cos\theta q_c(t)] \qquad (9)$$

where G_c and q_c are given by

$$G_c = I_c(\theta_0, \phi_0) \qquad (10a)$$
$$q_c = I_c(\theta, \phi)\cos\theta_0 = I_c(\theta_0, \phi_0)\cos\theta_0\delta(\theta - \theta_0)\delta(\phi - \phi_0) \qquad (10b)$$

In Eq. (10b), δ is the Dirac delta function defined as

$$\delta(\theta - \theta_0) = \begin{cases} 1, & \text{for } \theta = \theta_0 \\ 0, & \text{for } \theta \neq \theta_0 \end{cases} \qquad (11)$$

In Eq. (10) above, I_c is given by

$$I_c(\theta, \phi, t) = I_c(\theta_0, \phi_0, t)\exp(-\beta ds_0)$$
$$\times \left[H\{\beta(ct - ds_0)\} - H\{\beta(ct - ds_0) - \beta ct_p\}\right]$$
$$\times \delta(\theta - \theta_0)\delta(\phi - \phi_0) \qquad (12)$$

where $ds_0 = dz/\cos\theta_0$ is the geometric distance in the direction Ω_0 of the collimated radiation and $t^* = \beta ct$ is the non-dimensional time. Eq. (12) can be written as

$$I_c(\theta, \phi, t^*) = I_c(\theta_0, \phi_0, t^*)\exp(-\beta ds_0)$$
$$\times \left[H\{(t^* - \beta ds_0)\} - H\{(t^* - \beta ds_0) - t_p^*\}\right]$$
$$\times \delta(\theta - \theta_0)\delta(\phi - \phi_0) \qquad (13)$$

In the above equations, H is the Heaviside function defined as

$$H(y) = \begin{cases} 1, & y > 0 \\ 0, & y < 0 \end{cases} \qquad (14)$$

Radiation travels with the speed of light c and hence takes some finite time to reach a particular location. Therefore, the time of arrival of the pulse at that point will depend upon its location. Moreover, at any location in the medium, I_c remains available only for the duration t_p^* (see Fig. 2). These effects are taken care, mathematically by the introduction of the Heaviside function in the above equations.

In Eq. (5), the source term S_d resulting from the diffuse radiation I_d is given by

$$S_d(t^*) = \kappa_a I_b(t^*) + \frac{\sigma_s}{4\pi}\int_{\Omega'=0}^{4\pi} I_d(t^*)p(\Omega, \Omega')\,d\Omega' \qquad (15)$$

In terms of G and q, for linear anisotropic phase function $p(\Omega, \Omega') = 1 + a\cos\theta\cos\theta'$, Eq. (15) is given by

$$S_d(t^*) = \kappa_a I_b(t^*) + \frac{\sigma_s}{4\pi}[G_d(t^*) + a\cos\theta q_d(t^*)] \qquad (16)$$

In Eq. (16), G_d and q_d are given by [34]

$$G_d(t^*) = \int_{\Omega=0}^{4\pi} I_d(t^*)\,d\Omega$$
$$= \int_{\phi=0}^{2\pi}\int_{\theta=0}^{\pi} I_d(\theta, \phi, t^*)\sin\theta\,d\theta\,d\phi$$
$$\approx \sum_{k=1}^{M_\phi}\sum_{l=1}^{M_\theta} I_d(\theta_l, \phi_k, t^*)2\sin\theta_l\sin\left(\frac{\Delta\theta_l}{2}\right)\Delta\phi_k \qquad (17)$$

where M_θ and M_ϕ are the number of discrete points considered over the complete span of the polar angle θ ($0 \leqslant \theta \leqslant \pi$) and azimuthal angle ϕ ($0 \leqslant \phi \leqslant 2\pi$), respectively.

$$q_d(t^*) = \int_{\Omega=0}^{4\pi} I_d(t^*)\cos\theta\,d\Omega$$
$$= \int_{\phi=0}^{2\pi}\int_{\theta=0}^{\pi} I_d(\theta, \phi, t^*)\cos\theta\sin\theta\,d\theta\,d\phi$$
$$\approx \sum_{k=1}^{M_\phi}\sum_{l=1}^{M_\theta} I_d(\theta_l, \phi_k, t^*)2\sin\theta_l\cos\theta_l\sin(\Delta\theta_l)\Delta\phi_k \qquad (18)$$

For a boundary having temperature T_w and emissivity ε_w, the boundary intensity $I_d(r_w, t^*)$ is given by and computed from

$$I_d(r_w, t^*)$$
$$= \frac{\varepsilon\sigma T_w^4}{\pi} + \left(\frac{1-\varepsilon}{\pi}\right) \int_{\hat{n}_w \cdot \hat{s} < 0} [I_{d,w}(t^*) + I_{c,w}(t^*)] \cos\theta \, d\Omega$$
$$\approx \frac{\varepsilon\sigma T_w^4}{\pi} + \left(\frac{1-\varepsilon}{\pi}\right) \sum_{k=1}^{M_\phi} \sum_{l=1}^{M_\theta/2} [I_{d,w}(\theta_l, \phi_k, t^*)$$
$$+ I_{c,w}(\theta_l, \phi_k, t^*)] \sin\theta_l \cos\theta_l \sin\Delta\theta_l \Delta\phi_k \qquad (19)$$

where in Eq. (19), the first and the second terms represent emitted and reflected components of the boundary intensity, respectively. The reflected term is composed of the irradiation due to diffuse and collimated radiation.

In terms of non-dimensional time t^*, the RTE given in Eq. (6) is now written as

$$\beta\frac{\partial I_d}{\partial t^*} + \frac{dI_d}{ds} + \beta I_d = S_t \qquad (20)$$

Using fully implicit backward differencing scheme in time, Eq. (20) can be written as

$$\beta\frac{I_d(t^*) - I_d(t^* - \Delta t^*)}{\Delta t^*} + \frac{dI_d(t^*)}{ds} + \beta I_d(t^*) = S_t(t^*) \qquad (21)$$

Eq. (21) can be written in a simplified form as

$$B\frac{dI_d(t^*)}{ds} + \beta I_d(t^*) = BS_t(t^*) + CI_d(t^* - \Delta t^*) \qquad (22)$$

where $B = \frac{\Delta t^*}{(1+\Delta t^*)}$ and $C = \frac{\beta}{1+\Delta t^*}$.

With expressions for the source terms, incident radiation and heat flux given above, Eq. (22) is the resulting RTE to be used in the analysis of transient radiative transfer problems in the DTM, the DOM and the FVM. In the following pages, we provide methodology to solve Eq. (22) in the three methods. It is to be noted that in the DOM, the discrete directions and their associated weights are generally taken from the tabulated values provided in several references [12,13]. Mishra et al. [34] have recently proposed a simple quadrature scheme for the DOM which is the same as that being used in the DTM and the FVM. In this, for a given number of rays, the intensity directions and their associated weights required for the calculation of the incident radiation G and heat flux q are computed using simple formulae given in Eqs. (17) and (18), respectively. Thus, the intensity directions, their weights and the quadratures used to compute G and q essentially remain the same in the DTM, the DOM and the FVM. The only difference in the three methods then is the procedure for the calculation of the intensities which is explained in the following pages.

2.1. Discrete transfer method (DTM) formulation

In the DTM, Eq. (22) for a discrete direction Ω^m in the optical coordinate $\tau = \beta s$ is written as

$$B\frac{dI_d^m(t^*)}{d\tau} + I_d^m(t^*) = \frac{BS_t^m(t^*)}{\beta} + \frac{C}{\beta}I_d^m(t^* - \Delta t^*) \qquad (23)$$

Multiplying Eq. (23) with the integrating factor $\exp\left(\frac{\tau}{B}\right)$ and then integrating this equation between the upstream point U and the downstream point D in the direction Ω of the intensity, we get

$$\int_{\tau^U}^{\tau^D} d\left[\exp\left(\frac{\tau}{B}\right)I_d^m(t^*)\right]$$
$$= \left(\frac{1}{\beta}\right)\int_{\tau^U}^{\tau^D} S_t^m(t^*)\exp\left(\frac{\tau}{B}\right)d\tau$$
$$+ \frac{1}{(1+\Delta t^*)B}\int_{\tau^U}^{\tau^D} I_d^m(t^* - \Delta t^*)\exp\left(\frac{\tau}{B}\right)d\tau \qquad (24)$$

If the optical distance $\Delta\tau = \tau^D - \tau^U$ between the downstream point D and the upstream point U and in a given direction Ω is small enough, and assuming that the source term $S_t(t^*)$ at the present time level and the intensity $I_d(t^* - \Delta t^*)$ at the previous time level are known, then in the DTM, intensity at the downstream point D is found from the following recursive relation:

$$I_d^{m,D}(t^*) = I_d^{m,U}(t^*)\exp\left(-\frac{\Delta\tau}{B}\right)$$
$$+ \frac{BS_{t,av}^m(t^*)}{\beta}\left[1 - \exp\left(-\frac{\Delta\tau}{B}\right)\right]$$
$$+ \frac{I_{d,av}^m(t^* - \Delta t^*)}{(1+\Delta t^*)}\left[1 - \exp\left(-\frac{\Delta\tau}{B}\right)\right] \qquad (25)$$

where in the above equation, $S_{t,av}^m(t^*)$ and $I_{d,av}^m(t^* - \Delta t^*)$ are the values at the exact middle of the path-leg between the upstream point U and the downstream point D. In a planar medium, these are the average of their values at the two points.

$$S_{t,av}^m(t^*) = \frac{1}{2}\left[S_t^{m,D}(t^*) + S_t^{m,U}(t^*)\right] \qquad (26)$$

$$I_{d,av}^m(t^* - \Delta t^*) = \frac{1}{2}\left[I_d^{m,D}(t^* - \Delta t^*) + I_d^{m,U}(t^* - \Delta t^*)\right] \qquad (27)$$

In the 2-D geometries, $S_{t,av}^m(t^*)$ and $I_{d,av}^m(t^* - \Delta t^*)$ can be found using the bilinear interpolation of their values known at the four points on the control surfaces.

The space marching and ray tracing procedures in the DTM for the transient studies are the same as that for the steady-state analysis. Details on these can be found in [35,36]. In the application of the DTM to the transient radiative transfer, the intensity, and hence the source terms, the incident radiation and the heat flux are all functions of time. In the time marching procedure, at the first time level, at every point in the solution space, $S_{t,av}^m$ is given a guess value and $I_{d,av}^m(t^* - \Delta t^*)$ is taken zero. At this time level, the angular distribution of intensity $I_d^m(t^*)$ is found using Eq. (25). With $I_d^m(t^*)$ distribution known, $I_{d,av}^m(t^* - \Delta t^*)$ at the previous time level $(t^* - \Delta t^*)$ is calculated using Eq. (27). For the subsequent time levels t^*, source term $S_{t,av}^m(t^* - \Delta t^*)$ of the previous time level

$(t^* - \Delta t^*)$ becomes the guess values. At every time level, iterations are made until the convergence of the source term values at all the points is achieved. The procedure is repeated until the signals in the form of heat fluxes at the boundaries become weak.

2.2. The discrete ordinate method (DOM) formulation

Eq. (22) for a discrete direction Ω^m is written as

$$B \frac{\mathrm{d}I_d^m(t^*)}{\mathrm{d}s} + \beta I_d^m(t^*) = B S_t^m + C I_d^m(t^* - \Delta t^*) \tag{28}$$

$$I_{d,P}^m(t^*) = \frac{\left[\frac{\mu^m A_{EW}}{\alpha_x} I_{d,W}^m(t^*) + \frac{\xi^m A_{NS}}{\alpha_y} I_{d,S}^m(t^*) + \frac{\eta^m A_{FB}}{\alpha_z} I_{d,B}^m(t^*) + V S_{t,P}^m(t^*) + \left(\frac{CV}{B}\right) I_{d,P}^m(t^* - \Delta t^*) \right]}{\frac{\mu^m A_E}{\alpha_x} + \frac{\xi^m A_N}{\alpha_y} + \frac{\eta^m A_F}{\alpha_z} + \left(\frac{\beta V}{B}\right)} \tag{33}$$

Eq. (28) in the Cartesian coordinate directions can be written as

$$B \left[\mu^m \frac{\mathrm{d}I_d^m(t^*)}{\mathrm{d}x} + \xi^m \frac{\mathrm{d}I_d^m(t^*)}{\mathrm{d}y} + \eta^m \frac{\mathrm{d}I_d^m(t^*)}{\mathrm{d}z} \right] + \beta I_d^m(t^*)$$
$$= B S_t^m + C I_d^m(t^* - \Delta t^*) \tag{29}$$

where μ^m, ξ^m and η^m are the direction cosines of the intensity in the direction Ω^m having index m. In the DOM proposed in [34], these are computed from

$$\mu^m = \sin \theta^m \cos \phi^m, \quad \xi^m = \sin \theta^m \sin \phi^m,$$
$$\eta^m = \cos \theta^m \tag{30}$$

Integrating Eq. (29) over the control volume and using the concept of the FVM for the computational fluid dynamics, Eq. (29) is written as

$$\left[I_{d,E}^m(t^*) - I_{d,W}^m(t^*) \right] A_{EW} \mu^m + \left[I_{d,N}^m(t^*) - I_{d,S}^m(t^*) \right] A_{NS} \xi^m$$
$$+ \left[I_{d,F}^m(t^*) - I_{d,B}^m(t^*) \right] A_{FB} \eta^m$$
$$= -\frac{\beta V}{B} I_{d,P}^m(t^*) + V S_{t,P}^m + \frac{CV}{B} I_{d,P}^m(t^* - \Delta t^*) \tag{31}$$

where A_{EW}, A_{NS} and A_{FB} are the areas of the x-, y- and z-faces of the control volume, respectively. In Eq. (31), I with suffixes E, W, N, S, F and B designate east, west, north, south, front and back control surface average intensities, respectively. On the right-hand side of Eq. (31), $V = \mathrm{d}x \times \mathrm{d}y \times \mathrm{d}z$ is the volume of the cell and $I_{d,P}^m$ and $S_{t,P}^m$ are

the intensities and source terms at the cell centre P, respectively.

In any discrete direction Ω^m, the cell-surface intensities are related to the cell-centre intensity $I_{d,P}^m$ as

$$I_{d,P}^m = \alpha_x I_{d,E}^m + (1 - \alpha_x) I_{d,W}^m = \alpha_y I_{d,N}^m + (1 - \alpha_y) I_{d,S}^m$$
$$= \alpha_z I_{d,F}^m + (1 - \alpha_z) I_{d,B}^m \tag{32}$$

where α is the finite-difference weighting factor. While marching from the first octant for which μ^m, ξ^m and η^m are all positive, $I_{d,P}^m$ in terms of known cell-surface intensities can be written as

where

$$A_{EW} = (1 - \alpha_x) A_E + \alpha_x A_W,$$
$$A_{NS} = (1 - \alpha_y) A_N + \alpha_y A_S, \tag{34}$$
$$A_{FB} = (1 - \alpha_z) A_F + \alpha_z A_B$$

are the averaged areas. When any one of the μ^m, ξ^m or η^m is negative, marching starts from other corners. In this case, a general expression of $I_{d,P}^m$ in terms of known intensities and source term can be written as

$$I_{d,P}^m(t^*) = \frac{\left[\frac{|\mu^m| A_x}{\alpha_x} I_{d,x_i}^m(t^*) + \frac{|\xi^m| A_y}{\alpha_y} I_{d,y_i}^m(t^*) + \frac{|\eta^m| A_z}{\alpha_z} I_{d,z_i}^m(t^*) + V S_{t,P}^m(t^*) + \left(\frac{CV}{B}\right) I_{d,P}^m(t^* - \Delta t^*) \right]}{\frac{|\mu^m| A_{x_e}}{\alpha_x} + \frac{|\xi^m| A_{y_e}}{\alpha_y} + \frac{|\eta^m| A_{z_e}}{\alpha_z} + \left(\frac{\beta V}{B}\right)} \tag{35}$$

where in Eq. (35), x_i, y_i and z_i suffixes over I_d^m are for the intensities entering the control volume through x-, y- and z-faces, respectively and A_x, A_y and A_z are given by

$$A_x = (1 - \alpha_x) A_{x_e} + \alpha_x A_{x_i}, \quad A_y = (1 - \alpha_y) A_{y_e} + \alpha_y A_{y_i},$$
$$A_{FB} = (1 - \alpha_z) A_{z_e} + \alpha_z A_{z_i} \tag{36}$$

In Eq. (36) A with suffixes x_i, y_i and z_i represent control surface areas through which intensities enter the control volume while A with suffixes x_e, y_e and z_e represent control surface areas through which intensities leave the control volume.

At any time level, the space marching procedure in the application of the DOM to the transient situation is the same as that of the steady-state radiative transport problems details of which can be found in [12,13,15]. In its application to the transient radiative transfer, the time marching procedure is the same as that of the DTM described before. Expressions for the source terms in the present work, the quadratures for angular integrations for calculation of the incident radiation and heat flux are the same in the three methods and these are given in Eqs. (17) and (18).

2.3. Finite volume method (FVM) formulation

Writing Eq. (22) for a discrete direction Ω^m and integrating it over the elemental solid angle $\Delta\Omega^m$, we get

$$B \int_{\Delta\Omega^m} \frac{\mathrm{d}I_d^m(t^*)}{\mathrm{d}s}\,\mathrm{d}\Omega + \int_{\Delta\Omega^m} \beta I_d^m(t^*)\,\mathrm{d}\Omega$$
$$= \int_{\Delta\Omega^m} \left[BS_t^m(t^*) + CI_d^m(t^* - \Delta t^*) \right]\mathrm{d}\Omega \tag{37}$$

In the Cartesian coordinate directions, Eq. (37) can be written as

$$B \left[\frac{\partial I_d^m(t^*)}{\partial x} D_x^m + \frac{\partial I_d^m(t^*)}{\partial y} D_y^m + \frac{\partial I_d^m(t^*)}{\partial z} D_z^m \right] + \beta I_d^m(t^*)$$
$$= \left[BS_t^m(t^*) + CI_d^m(t^* - \Delta t^*) \right]\Delta\Omega^m \tag{38}$$

If $\hat{n}$ is the outward normal to a surface, then D^m is given by

$$D^m = \int_{\Delta\Omega^m} (\hat{n} \cdot \hat{s}^m)\,\mathrm{d}\Omega \tag{39}$$

where $\hat{s}^m = (\sin\theta^m \cos\phi^m)\hat{i} + (\sin\theta^m \sin\phi^m)\hat{j} + (\cos\theta^m)\hat{k}$. When $\hat{n}$ is pointing towards one of the positive coordinate directions, D_x^m, D_y^m and D_z^m are given by

$$D_x^m = \int_{\Delta\Omega^m} \sin\theta \cos\phi\,\mathrm{d}\Omega$$
$$= \int_{\phi^m - \frac{\Delta\phi^m}{2}}^{\phi^m + \frac{\Delta\phi^m}{2}} \int_{\theta^m - \frac{\Delta\theta^m}{2}}^{\theta^m + \frac{\Delta\theta^m}{2}} \cos\phi \sin^2\theta\,\mathrm{d}\theta\,\mathrm{d}\phi$$
$$= \cos\phi^m \sin\left(\frac{\Delta\phi^m}{2}\right)[\Delta\theta^m - \cos 2\theta^m \sin(\Delta\theta^m)] \tag{40a}$$

$$D_y^m = \int_{\Delta\Omega^m} \sin\theta \sin\phi\,\mathrm{d}\Omega$$
$$= \int_{\phi^m - \frac{\Delta\phi^m}{2}}^{\phi^m + \frac{\Delta\phi^m}{2}} \int_{\theta^m - \frac{\Delta\theta^m}{2}}^{\theta^m + \frac{\Delta\theta^m}{2}} \sin\phi \sin^2\theta\,\mathrm{d}\theta\,\mathrm{d}\phi$$
$$= \sin\phi^m \sin\left(\frac{\Delta\phi^m}{2}\right)[\Delta\theta^m - \cos 2\theta^m \sin(\Delta\theta^m)] \tag{40b}$$

$$D_z^m = \int_{\Delta\Omega^m} \cos\theta\,\mathrm{d}\Omega$$
$$= \int_{\phi^m - \frac{\Delta\phi^m}{2}}^{\phi^m + \frac{\Delta\phi^m}{2}} \int_{\theta^m - \frac{\Delta\theta^m}{2}}^{\theta^m + \frac{\Delta\theta^m}{2}} \cos\theta \sin\theta\,\mathrm{d}\theta\,\mathrm{d}\phi$$
$$= \sin\theta^m \cos\theta^m \sin(\Delta\theta^m)\Delta\phi^m \tag{40c}$$

For $\hat{n}$ pointing towards the negative coordinate directions, signs of D_x^m, D_y^m and D_z^m are opposite to what are obtained from Eq. (40).

In Eq. (38), $\Delta\Omega^m$ is given by

$$\Delta\Omega^m = \int_{\Delta\Omega^m} \mathrm{d}\Omega = \int_{\phi^m - \frac{\Delta\phi^m}{2}}^{\phi^m + \frac{\Delta\phi^m}{2}} \int_{\theta^m - \frac{\Delta\theta^m}{2}}^{\theta^m + \frac{\Delta\theta^m}{2}} \sin\theta\,\mathrm{d}\theta\,\mathrm{d}\phi$$
$$= 2 \sin\theta^m \sin\left(\frac{\Delta\theta^m}{2}\right)\Delta\phi^m \tag{41}$$

Integrating Eq. (38) over the control volume and using the concept of the FVM for the computational fluid dynamics, we get

$$\left[I_{d,E}^m(t^*) - I_{d,W}^m(t^*) \right]A_{EW}D_x^m + \left[I_{d,N}^m(t^*) - I_{d,S}^m(t^*) \right]A_{NS}D_y^m$$
$$+ \left[I_{d,F}^m(t^*) - I_{d,B}^m(t^*) \right]A_{FB}D_z^m$$
$$= \left[-\frac{\beta V}{B} I_{d,P}^m(t^*) + VS_{t,P}^m + \frac{CV}{B} I_{d,P}^m(t^* - \Delta t^*) \right]\Delta\Omega^m \tag{42}$$

With the procedure similar to the DOM given before, the general form of the cell-centre intensities $I_{d,P}^m(t^*)$ in terms of known cell-surface intensities can be written as

$$I_{d,P}^m(t^*) = \frac{\left[\frac{|D_x^m|A_x}{\alpha_x} I_{d,x_i}^m(t^*) + \frac{|D_y^m|A_y}{\alpha_y} I_{d,y_i}^m(t^*) + \frac{|D_z^m|A_z}{\alpha_z} I_{d,z_i}^m(t^*) + (V\Delta\Omega^m)S_{t,P}^m(t^*) + \left(\frac{CV\Delta\Omega^m}{B}\right)I_{d,P}^m(t^* - \Delta t^*) \right]}{\frac{|D_x^m|A_{x_e}}{\alpha_x} + \frac{|D_y^m|A_{y_e}}{\alpha_y} + \frac{|D_z^m|A_{z_e}}{\alpha_z} + \left(\frac{\beta V\Delta\Omega^m}{B}\right)} \tag{43}$$

where meanings of the various terms in Eq. (43) are the same as that in the DOM formulation.

The space marching in the FVM are the same as that of the DOM and the time marching procedure in the three methods are the same.

3. Results and discussion

The DTM, the DOM and the FVM formulations presented above are valid for an absorbing, emitting and scattering 3-D medium with diffuse-gray boundaries at arbitrary temperatures. To study primarily the effect of a square short-pulse collimated radiation, the emissions from the medium and its boundaries are neglected, and accordingly they are assumed cold. Thus in the above formulations, emission from the medium $I_b = 0$ and the boundary intensities are also zero. Further to simplify the situation, a planar medium with unity thickness ($Z = 1$ m) and black boundaries is considered (Fig. 2). The pulse-width and angle of incidence of the collimated radiation at the top boundary could be arbitrary.

While solving the problem, intensity I and heat flux values $q_t = q_c + q_d$ are non-dimensionalized with the maximum value (corresponding to normal incidence) of the collimated radiation I_c and the heat flux q_c, respectively.

Thus, in the problem under consideration, the magnitude of I_c is also arbitrary.

$$I^*(t^*) = \frac{I(t^*)}{I_c},$$
$$q_t^*(t^*) = \frac{q_c(t^*) + q_d(t^*)}{q_{c,max}} = \frac{q_c(t^*) + q_d(t^*)}{I_c} \qquad (44)$$

In the study of radiative transfer caused by a short-pulse laser irradiation, the time dependent transmittance $q_{tr}^*(t^*)$ and reflectance $q_{ref}^*(t^*)$ signals are the two quantities that provide specific information about the medium. Transmittance is defined as the net radiative heat flux emerging out of the medium due to transmission, and with reference to a planar medium (Fig. 2), it is the net radiative heat flux at the bottom boundary ($z = 0.0$). Reflectance is the net radi-

ative heat flux at the boundary which is subjected to the laser irradiation, and in the present case, it is the reflected heat flux at the top boundary ($z = Z$). In the following pages, effects of optical properties of the medium such as the extinction coefficient β, the scattering albedo ω and the anisotropy factor a on transmittance $q_{tr}^*(t^*)$ and reflectance $q_{ref}^*(t^*)$ signals are studied and compared in the DTM, the DOM and the FVM. Further, effects of the pulse-width and the angle of incidence of the collimated radiation on these signals are also studied.

For a grid-independent situation, a maximum of 500 equal size control volumes and for a ray-independent situation, 40 equally spaced directions were considered in the three methods. The total observed time span was divided into 1000 equal steps. At a given time level, convergence
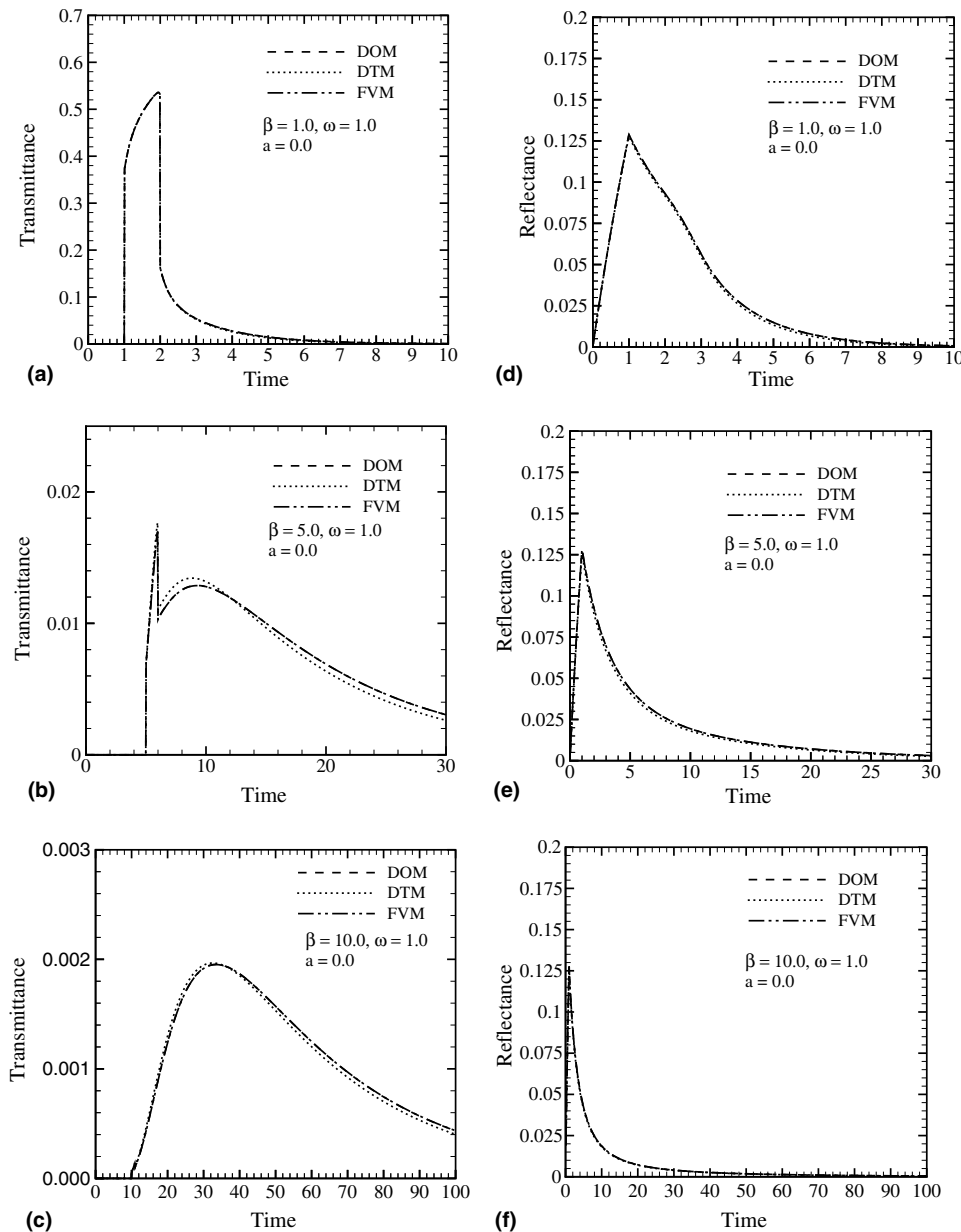

Fig. 3. Effect of the extinction coefficient β on transmittance $q_{tr}^*(t^*)$ and reflectance $q_{ref}^*(t^*)$ signals.

was assumed to have been achieved when change in source term $S(t^*)$ values at all points for the two consecutive iteration levels did not exceed 1×10^{-7}.

In Figs. 3–5, $q_{tr}^*(t^*)$ and $q_{ref}^*(t^*)$ signals computed using the DTM, the DOM and the FVM have been shown for non-dimensional pulse-width $t_p^* = 1.0$ and normal incidence $\theta_0 = 0°$. Results for variable angle of incidence θ_0 and pulse-width t_p^* have been shown in Figs. 6 and 7, respectively.

Effects of the extinction coefficient β on $q_{tr}^*(t^*)$ and $q_{ref}^*(t^*)$ signals have been shown in Fig. 3a–f, respectively. These effects of β have been shown for an absorbing and isotropically scattering ($a = 0.0$) medium with $\omega = 1.0$.

It can be seen that the $q_{tr}^*(t^*)$ signals appear at $t^* = t_s^* = \frac{\beta Z}{\cos \theta_0} = \beta$ and $q_{ref}^*(t^*)$ signals remain available since the start of the process. With increase in β, the peaks of $q_{tr}^*(t^*)$ decrease while those of the $q_{ref}^*(t^*)$ remain unchanged. But with increase in β, both signals last longer. This is because the mean free-path decreases with increase in β, and thus radiation is unable to percolate quickly through the medium. It is further seen from Fig. 3a–c that after their appearances, $q_{tr}^*(t^*)$ and $q_{ref}^*(t^*)$ undergo a noticeable change at $t^* = t_s^* + t_p^*$ and $t^* = t_p^*$, respectively. In case of $q_{tr}^*(t^*)$, this change is more prominent for lower β (Fig. 3a). This is because with increase in β, the diffuse radiation scores over the collimated component, and after $t^* = t_s^* + t_p^*$, $q_{tr}^*(t^*)$ is composed of only the diffuse

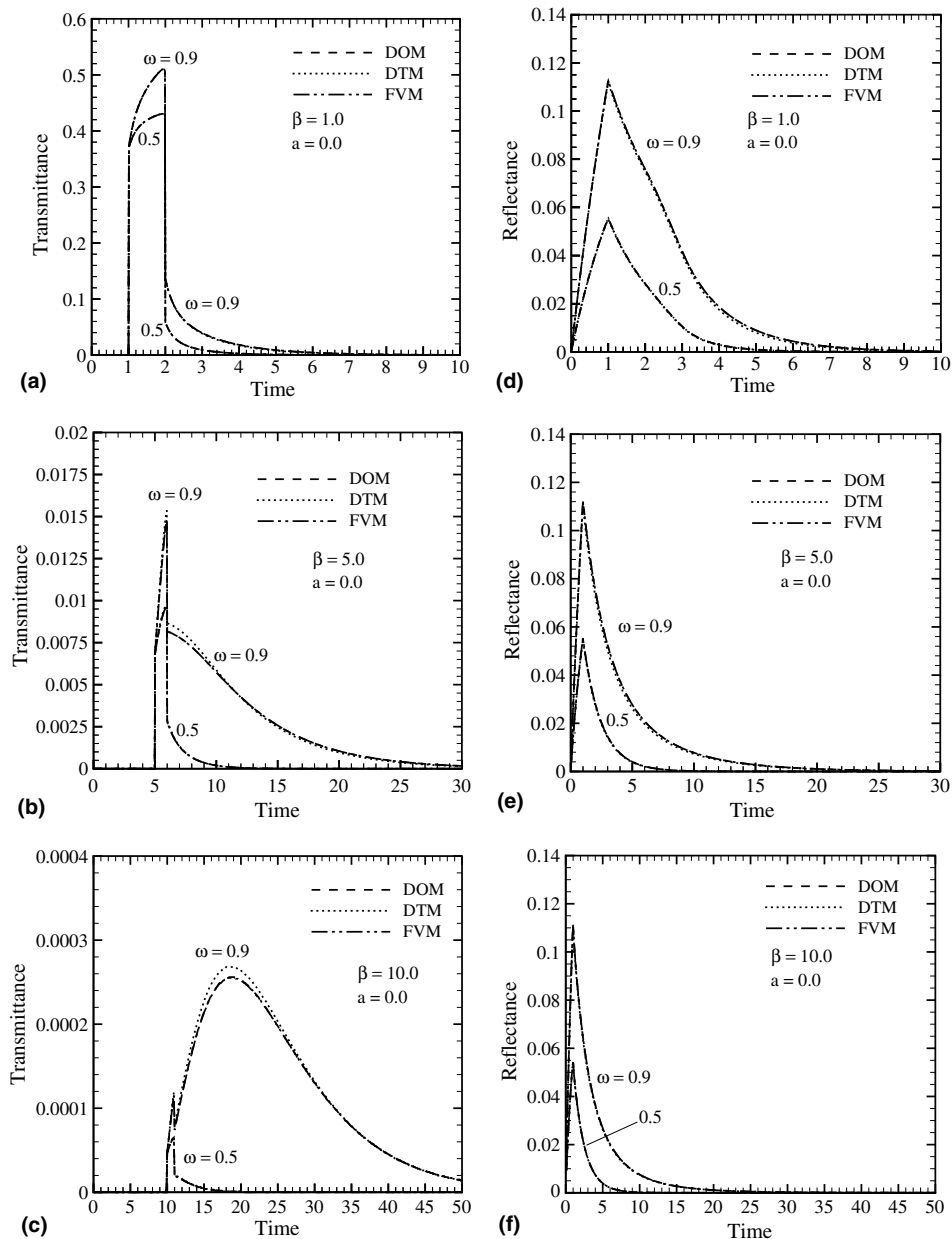Fig. 4. Effect of scattering albedo ω on transmittance $q_{tr}^*(t^*)$ and reflectance $q_{ref}^*(t^*)$ signals.
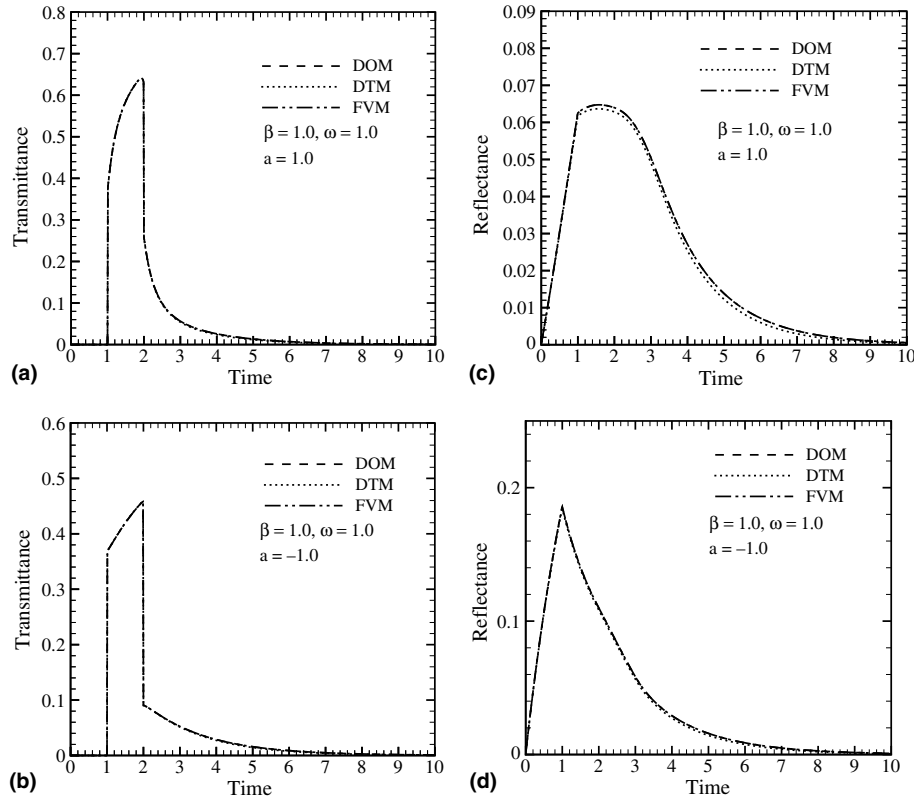
Fig. 5. Effect of anisotropy factor a on transmittance $q_{tr}^*(t^*)$ and reflectance $q_{ref}^*(t^*)$ signals.

component. The same is true for the $q_{tr}^*(t^*)$ in which this happens after $t^* = t_p^*$.

It can be seen that for all the cases, results of the DTM, the DOM and the FVM compare very well with each other.

The effects of the scattering albedo ω on $q_{tr}^*(t^*)$ and $q_{ref}^*(t^*)$ have been shown in Fig. 4a–c and d–f respectively for $a = 0.0$. These effects have been shown for $\omega = 0.9$ and 0.5. It is seen from the figures that the dependence of $q_{tr}^*(t^*)$ on ω is relatively more pronounced for higher values of β (Fig. 4c). The effect of ω on $q_{ref}^*(t^*)$ is the same for all β. For a given β, with decrease in ω, the peaks of both the signals decrease and they last for a shorter duration. This is because for a higher value of ω, radiation suffers multiple scattering in the medium and is hence constrained to last longer. The time at which change in the peak values of both the signals occurs is independent of ω.

For results presented in Fig. 4a–f, it is seen that results of the DTM, the DOM and the FVM match very well with each other.

The effects the anisotropy a on $q_{tr}^*(t^*)$ and $q_{ref}^*(t^*)$ have been shown in Fig. 5a, b and c, d, respectively for $\omega = 1.0$ and $\beta = 1.0$. These effects have been shown for 100% forward scattering $a = +1.0$ and 100% backward scattering $a = -1.0$. It can be seen that the peak of $q_{tr}^*(t^*)$ is more in case of the forward scattering $a = +1.0$. However, opposite is the case with $q_{ref}^*(t^*)$. This trend is attributed to the fact that for $a = +1.0$, more energy is scattered in the direction of travel. Hence the peak value of $q_{tr}^*(t^*)$ is

more while that of $q_{ref}^*(t^*)$ is less than its values in the backward scattering case $a = -1.0$. The DTM, the DOM and the FVM results are seen to compare very well with each other.

Effect of the angle of incidence θ_0 on $q_{tr}^*(t^*)$ and $q_{ref}^*(t^*)$ has been shown in Fig. 6a–f. For $\omega = 1.0$ and $a = 0.0$, $q_{tr}^*(t^*)$ and $q_{ref}^*(t^*)$ are shown for three values of β. For every β, results have been shown for $\theta_0 = 0°$, 45°, and 60°. It is observed from Fig. 6a–f that the peak values decrease with an increase in θ_0. This is because with increase in θ_0 according to Eq. (10b), the radiative energy penetrating the medium through the top boundary decreases. Further it is seen that in the case of $q_{tr}^*(t^*)$, the time of start of the signal $t^* = t_s^* = \frac{\beta Z}{\cos \theta_0} = \frac{\beta}{\cos \theta_0}$ is more for higher values of θ_0. The DTM, the DOM and the FVM results are seen to be in good agreement.

Effect of the pulse-width t_p^* on $q_{tr}^*(t^*)$ and $q_{ref}^*(t^*)$ are shown in Fig. 7a and b, respectively. For $\theta_0 = 0°$, $\beta = 1.0$, $\omega = 1.0$ and $a = 0.0$, these results are shown for $t_p^* = 1.0$, 5.0 and 10.0. It is seen that the peak values of $q_{tr}^*(t^*)$ and $q_{ref}^*(t^*)$ increase with increase in t_p^*. This is for the reason that with increase in t_p^*, the medium receives energy for the longer duration. Further it can be observed that in the duration of the pulse-width, with increase in t_p^*, $q_{tr}^*(t^*)$ and $q_{ref}^*(t^*)$ asymptotically reach constant values. This is true because for a pulse-width $t_p^* \rightarrow \infty$, the top boundary will receive radiation continuously and hence the situation becomes that of the steady-state in which
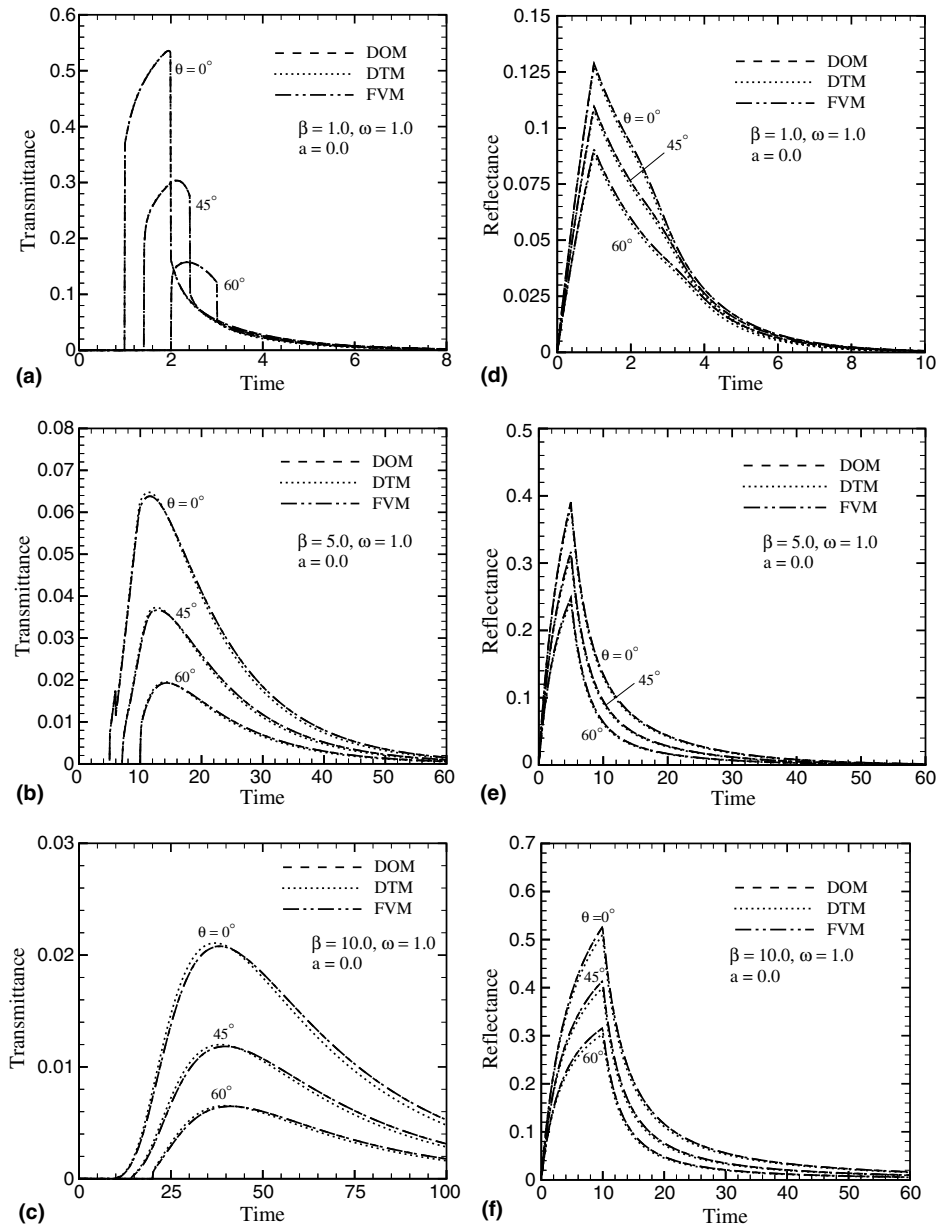
Fig. 6. Effect of angle of incidence on transmittance $q_{\mathrm{tr}}^*(t^*)$ and reflectance $q_{\mathrm{ref}}^*(t^*)$ signals.
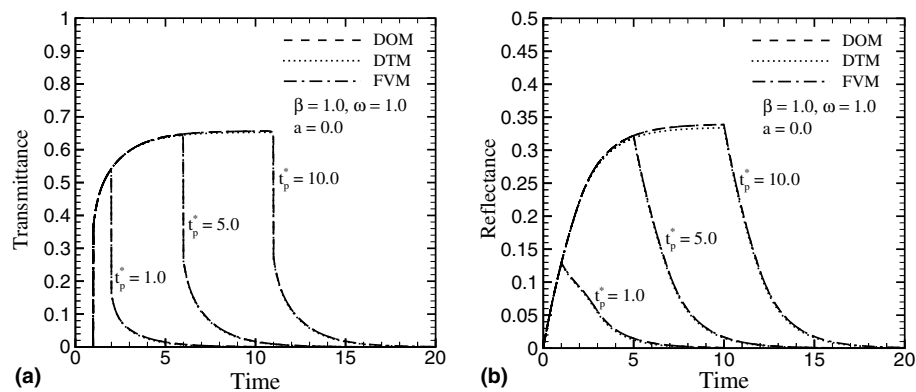

Fig. 7. Effect of pulse-width t_{p}^* on transmittance $q_{\mathrm{tr}}^*(t^*)$ and reflectance $q_{\mathrm{ref}}^*(t^*)$ signals.

Table 1
Comparison of the CPU times (in second) of the DTM, the DOM and the FVM

Number of control volumes	Number of rays	CPU times (s)		
		DTM	DOM	FVM
100	40	165.31	85.67	155.80
200	40	529.39	201.02	352.94
300	40	605.22	381.19	486.31
400	40	840.40	465.77	773.91
500	40	959.38	620.00	923.00
500	10	537.29	328.97	380.91
500	20	612.16	448.89	550.80
500	30	809.84	517.92	750.70
500	45	1056.83	724.66	939.19

$q_{tr}^*(t^*)$ and $q_{ref}^*(t^*)$ will have constant values. In this case also, the DTM, the DOM and the FVM results have a close match.

3.1. Comparison of CPU times

Having found that in all the cases, the DTM, the DOM and the FVM results are in good agreement with each other, we next study the computational efficiency of the three methods. For $\beta = 1.0$, $\omega = 1.0$, $a = 0.0$ and $\theta_0 = 0°$, the CPU times (in second) in the three methods are compared in Table 1. All runs were taken on the IBM Thinkpad, Model R40, Mobile Intel Pentium 4, 2.0 GHz, 256 MB RAM at 266 MHz.

It is seen from Table 1 that the DOM is computationally the most efficient. Since the FVM and the DOM procedures are exactly the same, except that the FVM spends extra time in integrating intensity over an elemental solid angle, the CPU time of the FVM is always higher than the DOM. However, this extra computation in the FVM has an advantage over the DOM in multidimensional geometries and in strongly anisotropically scattering medium in which case the ray effect is more pronounced [36]. The DTM spends much time in ray tracing and source term evaluation, hence its computational time is always more than the DOM and the FVM.

4. Conclusions

A general formulation of the DTM, the DOM and the FVM to study the transmittance and reflectance signals caused by the irradiation of a short-pulse laser was presented. The formulations in the three methods were similar in the sense that the intensity directions and the quadratures to compute incident radiation and heat flux were the same. The time marching procedure in the three methods was also the same. The DTM differed from the DOM and the FVM in the ray tracing approach. To validate the formulation and to compare the results of the three methods, a planar absorbing-scattering cold medium with black boundary was considered. The transmittance and reflectance signals were studied and compared for different val-

ues of the extinction coefficient, the scattering albedo, the anisotropy factor, the angle of incidence and the pulse-width of the square pulse. These parameters were found to have significant bearings on the temporal variations of these signals. In all the cases, the results from the three methods were found to match very well with each other. Computationally, the DOM was found to be the most efficient.

References

[1] M.J.C. Gemert, J.J. Wetch, Clinical use of laser–tissue interaction, JEEE Eng. Med. Biol. Mag. 8 (4) (1989) 10–13.

[2] F. Liu, K.M. Yoo, R.R. Alfano, Ultra-fast laser pulse transmission and imaging through biological tissues, Appl. Opt. 32 (1993) 554–558.

[3] Y. Yamada, Light–Tissue Interaction and Optical Imaging in Bio-Medicine, vol. 6, Beggel House, New York, 1995, pp. 1–59.

[4] M. Sakami, K. Mitra, T. Vo-Dinh, Analysis of short-pulse laser photon transport through tissues for optical tomography, Opt. Lett. 27 (2002) 336–338.

[5] R.E. Walker, J.W. Mclean, Lidar equation for turbid media with pulse stretching, Appl. Opt. 38 (1999) 2384–2397.

[6] K. Mitra, J.H. Churnside, Transient radiative transfer equation applied to oceanographic lidar, Appl. Opt. 38 (1999) 889–895.

[7] S.A. Prahl, M.J.C. Van Gemert, A.J. Welch, Determining the optical properties of turbid media by adding-doubling method, Appl. Opt. 32 (1993) 559–568.

[8] J. Noack, A. Vogel, Single-shot spatially resolved characterization of laser induced shock waves in water, Appl. Opt. 37 (1998) 4092–4099.

[9] C.L. Tien, A. Majumdar, F.M. Gerner, Microscale Energy Transfer, Taylor and Francis, Washington, DC, 1997.

[10] S. Kumar, K. Mitra, Microscale aspects of thermal radiation transport and laser applications, Adv. Heat Transfer 33 (1999) 187–294.

[11] K.J. Grant, J.A. Piper, D.J. Ramsay, K.L. Williams, Pulse lasers in particle detection and sizing, Appl. Opt. 33 (1993) 416–417.

[12] M.F. Modest, Radiative Heat Transfer, second ed., Academic Press, New York, 2003.

[13] R. Siegel, J. Howell, Thermal Radiation Heat Transfer, fourth ed., Taylor & Francis, New York, 2002.

[14] N.G. Shah, A new method of computation of radiation heat transfer in combustion chambers, Ph.D. Thesis, Imperial College, University of London, England, 1979.

[15] W.A. Fiveland, Discrete-ordinates solution of the radiative transport equation for rectangular enclosures, J. Heat Transfer 106 (1984) 699–706.

[16] J.C. Chai, S.V. Patankar, Finite volume method for radiation heat transfer, Adv. Numer. Heat Transfer 2 (2000) 110–135.

[17] S. Kumar, K. Mitra, Y. Yamada, Hyperbolic damped-wave models for transient light-pulse propagation in scattering media, Appl. Opt. 35 (1996) 3372–3378.

[18] K. Mitra, M.S. Lai, S. Kumar, Transient radiation transport in participating media within a rectangular enclosure, J. Thermophys. Heat Transfer 11 (1997) 409–414.

[19] Z.M. Tan, P.F. Hsu, An integral formulation of transient radiative transfer, J. Heat Transfer 123 (2001) 466–475.

[20] Z.M. Tan, P.-f. Hsu, Transient radiative transfer in three-dimensional homogeneous and non homogeneous participating media, J. Quant. Spectros. Radiat. Transfer 73 (2002) 181–194.

[21] C.Y. Wu, S.H. Wu, Integral equation formulation for transient radiative transfer in an anisotropically scattering medium, Int. J. Heat Mass Transfer 122 (2000) 818–822.

[22] C.Y. Wu, N.R. Ou, Differential approximation for transient radiative transfer through a participating medium exposed to collimated radiation, J. Quant. Spectros. Radiat. Transfer 73 (2002) 111–120.

[23] H. Schweiger, A. Oliva, M. Costa, C.D.P. Segarra, A Monte Carlo method for the simulation of transient radiation heat transfer: application to compound honeycomb transparent insulation, Numer. Heat Transfer B 35 (2001) 113–136.

[24] Z. Guo, J. Aber, B.A. Garetz, S. Kumar, Monte Carlo simulation and experiments of pulsed radiative transfer, J. Quant. Spectros. Radiat. Transfer 73 (2002) 159–168.

[25] Z. Guo, S. Kumar, K.C. San, Multi-dimensional Monte Carlo simulation of short-pulsed transport in scattering media, J. Thermophys. Heat Transfer 14 (2000) 504–511.

[26] Z. Guo, S. Kumar, Discrete-ordinates solution of short-pulsed laser transport in two-dimensional turbid media, Appl. Opt. 40 (2001) 3156–3163.

[27] M. Sakami, K. Mitra, P.-f. Hsu, Analysis of light-pulse transport through two-dimensional scattering and absorbing media, J. Quant. Spectros. Radiat. Transfer 73 (2002) 169–179.

[28] Z. Guo, S. Kumar, Three-dimensional discrete ordinates method in transient radiative transfer, J. Thermophys. Heat Transfer 16 (2002) 289–296.

[29] P. Rath, S.C. Mishra, P. Mahanta, U.K. Saha, K. Mitra, Discrete transfer method applied to transient radiative problems in participating medium, Numer. Heat Transfer, Part A 44 (2003) 183–197.

[30] Z. Guo, S. Kumar, Radiation element method for hyperbolic radiative transfer in plane—parallel inhomogeneous media, Numer. Heat Transfer B 39 (4) (2001) 371–387.

[31] J.C. Chai, One-dimensional transient radiative heat transfer modeling using a finite volume method, Numer. Heat Transfer B 44 (2003) 187–208.

[32] J.C. Chai, P.-f. Hsu, Y.C. Lam, Three-dimensional transient radiative transfer modeling using the finite volume method, J. Quant. Spectros. Radiat. Transfer 86 (2004) 299–313.

[33] K. Mitra, S. Kumar, Development and comparisons of models for light-pulse transport through scattering-absorbing media, Appl. Opt. 38 (1999) 188–196.

[34] S.C. Mishra, H.K. Roy, N. Misra, Discrete ordinate method with a new and a simple quadrature scheme, J. Quant. Spectros. Radiat. Transfer, in press, doi:10.1016/j.jqsrt.2005.11.018.

[35] S.C. Mishra, P. Talukdar, D. Trimis, F. Durst, Computational efficiency improvements of the radiative transfer problems with or without conduction—a comparison of the collapsed dimension method and the discrete transfer method, Int. J. Heat Mass Transfer 46 (2003) 3083–3095.

[36] P.J. Coelho, M.G. Carvalho, A conservative formulation of the discrete transfer method, J. Heat Transfer 119 (1997) 118–128.